NEOPLASIA
www.neoplasia.com

Volume 15 Number 11 November 2013 pp. 1292–1300 1292

ETV6/RUNX1 Induces Reactive Oxygen Species and Drives the Accumulation of DNA Damage in B Cells[1,2]

Hans-Peter Kantner[*,3], Wolfgang Warsch[†,3], Alessio Delogu[*,4], Eva Bauer[*], Harald Esterbauer[‡], Emilio Casanova[*], Veronika Sexl[†] and Dagmar Stoiber[*,§]

*Ludwig Boltzmann Institute for Cancer Research, Vienna, Austria; [†]Institute of Pharmacology and Toxicology, Veterinary University of Vienna, Vienna, Austria; [‡]Clinical Institute of Laboratory Medicine, Medical University of Vienna, Vienna, Austria; [§]Institute of Pharmacology, Medical University of Vienna, Vienna, Austria

Abstract

The t(12;21)(p13;q22) chromosomal translocation is the most frequent translocation in childhood B cell precursor–acute lymphoblastic leukemia and results in the expression of an ETV6/RUNX1 fusion protein. The frequency of *ETV6/RUNX1* fusions in newborns clearly exceeds the leukemia rate revealing that additional events occur in *ETV6/RUNX1*–positive cells for leukemic transformation. Hitherto, the mechanisms triggering these second hits remain largely elusive. Thus, we generated a novel *ETV6/RUNX1* transgenic mouse model where the expression of the fusion protein is restricted to $CD19^+$ B cells. These animals harbor regular B cell development and lack gross abnormalities. We established stable pro-B cell lines carrying the *ETV6/RUNX1* transgene that allowed us to investigate whether ETV6/RUNX1 itself favors the acquisition of second hits. Remarkably, these pro-B cell lines as well as primary bone marrow cells derived from *ETV6/RUNX1* transgenic animals display elevated levels of reactive oxygen species (ROS) as tested with *ETV6/RUNX1* transgenic dihydroethidium staining. In line, intracellular phospho-histone H2AX flow cytometry and comet assay revealed increased DNA damage indicating that ETV6/RUNX1 expression enhances ROS. On the basis of our data, we propose the following model: the expression of ETV6/RUNX1 creates a preleukemic clone and leads to increased ROS levels. These elevated ROS favor the accumulation of secondary hits by increasing genetic instability and double-strand breaks, thus allowing preleukemic clones to develop into fully transformed leukemic cells.

Neoplasia (2013) 15, 1292–1300

Introduction

The *ETV6/RUNX1* (*TEL/AML1*) fusion gene is the most common chromosomal alteration in pediatric cancer and occurs in approximately 25% of children with B cell precursor–acute lymphoblastic leukemia (BCP-ALL) [1,2]. The t(12;21)(p13;q22) chromosomal translocation results in the fusion of two critical regulators of hematopoiesis, bringing together the 5′ portion of the *ETV6* (*TEL*) gene on chromosome 12p13 and nearly the entire *RUNX1* (*AML1*) gene on chromosome 21q22 [3,4]. Persuasive evidence that clearly shows the presence of the *ETV6/RUNX1* fusion already prenatally and defines it as an early and initiating mutation is available. These insights were obtained from studies of identical twins with concordant ALL [5] and retrospective screening of archived neonatal blood spots of children diagnosed with ALL [6]. The early arise of the translocation indicates that it presents the first event ("hit") in the process of leukemogenesis creating a

Abbreviations: BCP-ALL, B cell precursor–acute lymphoblastic leukemia; ROS, reactive oxygen species; DSB, double-strand break; DHE, dihydroethidium; *E/R^{fg}*, *ETV6/RUNX1* transgene

Address all correspondence to: Dagmar Stoiber, PhD, Ludwig Boltzmann Institute for Cancer Research, Waehringerstrasse 13A, A-1090 Vienna, Austria.
E-mail: dagmar.stoiber@lbicr.lbg.ac.at

[1]Financial support for this project was provided by the St Anna Kinderkrebsforschung, Children's Cancer Research Institute, financing the position of H.-P.K. and E.B. Further support came from the Austrian Science Fund Fonds zur Förderung der wissenschaftlichen Forschung (FWF) SFB-F28 to V.S. The authors declare no conflict of interests.

[2]This article refers to supplementary materials, which are designated by Figures W1 to W4 and are available online at www.neoplasia.com.

[3]These authors contributed equally.

[4]Current address: Dept of Neuroscience, Institute of Psychiatry, King's College London, London, United Kingdom.

Received 9 July 2013; Revised 4 October 2013; Accepted 7 October 2013

DOI 10.1593/neo.131310

preleukemic clone. This is further supported by the fact that the fusion gene may be present for up to 10 years before leukemia diagnosis [7,8]. Secondary genetic events are clearly required for the clinical manifestation of the leukemia that evolves from an ETV6/RUNX1$^+$ preleukemic clone that is characterized by the surface markers CD34$^+$CD38$^{-/low}$CD19$^+$ [9,10].

At the time point of diagnosis, *ETV6/RUNX1*$^+$ ALL is characterized by multiple copy number alterations [11,12]. So far, it is elusive how the presence of ETV6/RUNX1 induces the acquisition of these additional genetic events during pathogenesis of BCP-ALL.

Genomic instability is one of the characteristics of transformed cells [13] and may arise from increased DNA damage and/or impaired DNA repair [14]. DNA damage occurs due to spontaneous decay but also results from exposure to radiation or certain chemicals. Reactive oxygen species (ROS) are chemically reactive molecules that participate in self-propagating reactions, and, if allowed to accumulate, they can cause oxidative damage to intracellular macromolecules, including DNA, proteins, and lipids [15]. The increased mutation rate in a variety of cancers has been attributed to the accumulation of ROS [16]. The capability of ROS to induce DNA double-strand breaks (DSBs) stresses the potential of ROS for triggering chromosomal aberrations [17–20]. Additionally to ROS-mediated mutagenesis, the expression of leukemia-associated fusion genes may interfere with DNA repair as convincingly demonstrated for breakpoint cluster region/Abelson 1 (BCR/ABL1) leukemia [21]. DNA repair is also disturbed in leukemic cells characterized by translocation products such as *RUNX1/ETO* (*AML1/ETO*) [22,23] and in cases of ETV6/RUNX1$^+$ leukemia [12]. ETV6/RUNX1$^+$ cells also display a disrupted spindle checkpoint that may result in aneuploidy [24].

In this study, we describe a novel mouse model where ETV6/RUNX1 expression is restricted to CD19$^+$ B lymphoid cells. In line with earlier reports [25–30], we did not observe leukemia formation in these animals. Here, we describe for the first time that the expression of ETV6/RUNX1 is associated with increased levels of ROS and the subsequent accumulation of DSBs, a prerequisite for mutagenesis. These findings suggest that the expression of ETV6/RUNX1 triggers mutagenesis through enhanced ROS production.

Design and Methods

Generation of a CD19$^+$ B Cell–Specific ETV6/RUNX1-Expressing Mouse

To generate a mouse that expresses ETV6/RUNX1 specifically in CD19$^+$ cells, the CD19 bacterial artificial chromosome (BAC) RP23-407K24 was used. For BAC modification, the building vector pQS-CD19 containing an *Eco*RI and *Nhe*I restriction site was used [31]. The human *ETV6/RUNX1* cDNA was amplified from an pMSCV-ETV6/RUNX1–internal ribosomal entry site (IRES)–green fluorescent protein (GFP) plasmid (a kind gift of O. Williams, University College London, Institute of Child Health, London, United Kingdom) using the primers 5′ GCGGAATTCATGTCTGAGACTCCTGCTCAG 3′ containing an *Eco*RI site and 5′ GCGGCTAGCTTAAGCGTAATCTGGAACATCGTATGGGTA 3′ containing an *Nhe*I site and a hemagglutinin (HA) tag. This fragment was inserted into the plasmid pQS-CD19 using *Eco*RI and *Nhe*I restriction sites. After *Not*I digestion, the linearized form of pQS-CD19-ETV6/RUNX1 was used to insert the ETV6/RUNX1-IRES-hCD2t expression cassette into the mouse CD19 BAC RP23-407K24 by standard BAC modification procedures as described earlier [32]. The expression cassette was thereby inserted into exon 1 of the CD19 BAC to express ETV6/RUNX1 and hCD2t under the control of the *Cd19* promotor. Upon recombination, the start codon (ATG) of the *Cd19* coding sequence in exon 1 is replaced by the ETV6/RUNX1-IRES-hCD2t-polyA expression cassette. Transcription from the *Cd19* promoter is terminated by a polyadenylation signal just after the *hCD2t* coding sequence. Furthermore, the inserted bicistronic cDNA is not in frame with the *Cd19* coding sequence. Transgenic mice were generated by injection of linearized BAC DNA at 1 ng/μl into pronuclei of C57BL/6×CBA F1 zygotes. The transgenic animals were backcrossed to C57BL/6 mice for seven generations. *ETV6/RUNX1* transgenic (E/R^{tg}) mice were genotyped using the following oligos: forward—5′ GCCAGACATTGTGGCATATG 3′ and reverse—5′ CGAGTCTTCCTCCATCCTGA 3′. Mice were kept at the animal facility at Research Institute of Molecular Pathology/Institute of Molecular Biotechnology (IMP/IMBA; Vienna, Austria). All animal experiments were carried out in accordance with protocols approved by the animal committee of the Medical University of Vienna and by the Federal Ministry of Science and Research.

Southern Blot Analysis

Twenty micrograms of tail genomic DNA of wt and E/R^{tg} littermates were digested with *Bam*HI, separated on a 1% agarose gel, transferred to a nylon membrane (Macherey-Nagel, Düren, Germany), and hybridized with a probe downstream of the insertion site of the ETV6/RUNX1-IRES-hCD2t expression cassette (amplification primers, forward—5′ GGTATCGAGGTAACCAGTCAACACCC 3′ and reverse—5′ GTACCCCACAGGACAGCCAAAGTGTGG 3′).

mRNA Expression Analysis and Semiquantitative Reverse Transcription–Polymerase Chain Reaction Analysis

Total RNA from bone marrow (BM) and spleen was isolated using TRIzol (TRI Reagent; Sigma-Aldrich, Vienna, Austria) and subsequently treated with DNase I (DNase I recombinant; Roche Diagnostics, Vienna, Austria). cDNA was prepared with RevertAid H Minus First Strand cDNA Synthesis Kit (Fermentas, St. Leon-Rot, Germany) using random hexamer primers. Sequences of primer pairs used during the course of the study (5′-3′) are given as follows: *ETV6/RUNX1*, forward—CTCTGTCTCCCCGCCTGAA and reverse—CGGCTCGTGCTGGCAT; mouse *Etv6*, forward—GATAGTGGATCCCAACGGACT and reverse—ACGTTTGTTCATCCAGCACTT; and mouse *Hprt*, forward—GATACAGGCCAGACTTTGTTG and reverse—GGTAGGCTGGCCTATAGGCT.

Blood Smears and Blood Parameters

Blood smears were stained with Hemacolor Rapid staining of blood smear staining set (Merck Millipore, Billerica, MA). Confocal images (original magnification, ×100) were taken using a Carl Zeiss (Oberkochen, Germany) Axio Imager.Z1 microscope. Blood parameters were measured from EDTA blood by scil Vet ABC (Gurnee, IL) according to the manufacturers' instructions.

Flow Cytometric Analysis

Single-cell suspensions were preincubated with anti-CD16/CD32 (24G2) antibody to prevent nonspecific Fc receptor–mediated

binding. Antibodies used for lineage determination included CD3e (145-2C11), Ter119 (Ter119), Gr-1 (RB6-8C5), CD11b (M1/70), and CD19 (1D3). An antibody against human CD2 (RPA 2.1; all BD Biosciences, San Jose, CA) as marker for ETV6/RUNX1 expression was used. Staining for free oxygen radicals was performed using dihydroethidium (DHE; Molecular Probes, Eugene, OR). For flow cytometric detection of phospho-histone H2AX (γH2AX; S139; Cell Signaling Technology; clone 20E3), B cells were fixed in paraformaldehyde (Sigma-Aldrich; 2%), permeabilized by exposure to ice-cold methanol (–20°C, 30 minutes), washed in phosphate-buffered saline containing 0.5% BSA (Sigma-Aldrich) and 0.2% Tween 20 (Sigma-Aldrich), and stained with an Alexa Fluor 647–conjugated γH2AX antibody (Cell Signaling Technology, Danvers, MA) for 60 minutes (room temperature). Subsequently, cells were washed and analyzed. Samples were acquired on a BD FACSCanto II FACS device (BD Biosciences), and data were analyzed with FlowJo software (TreeStar, Ashland, OR).

Protein Analysis

Protein expression has been determined from the fetal liver–derived CD19$^+$ B cell lines of wt and E/R^{tg} mice. Cells were lysed in a buffer containing protease and phosphatase inhibitors [25 mM Hepes (pH 7.5), 150 mM NaCl, 10 mM EDTA, 0.1% Tween 20, 0.5% NP-40, 10 mM β-glycerophosphate, 40 µl/ml protease inhibitor cocktail (Roche, Basel, Switzerland), 0.1 mM PMSF, 0.1 mM $NaVO_4$, and 1 mM DTT]. The protein concentration was determined by Bio-Rad protein assay kit as recommended by the manufacturer (Bio-Rad Laboratories, Hercules, CA). ETV6/RUNX1 was immunoprecipitated of 2 mg of cell lysate using an anti-RUNX1 antibody (N-20; Santa Cruz Biotechnology, Dallas, TX) and probed with a polyclonal

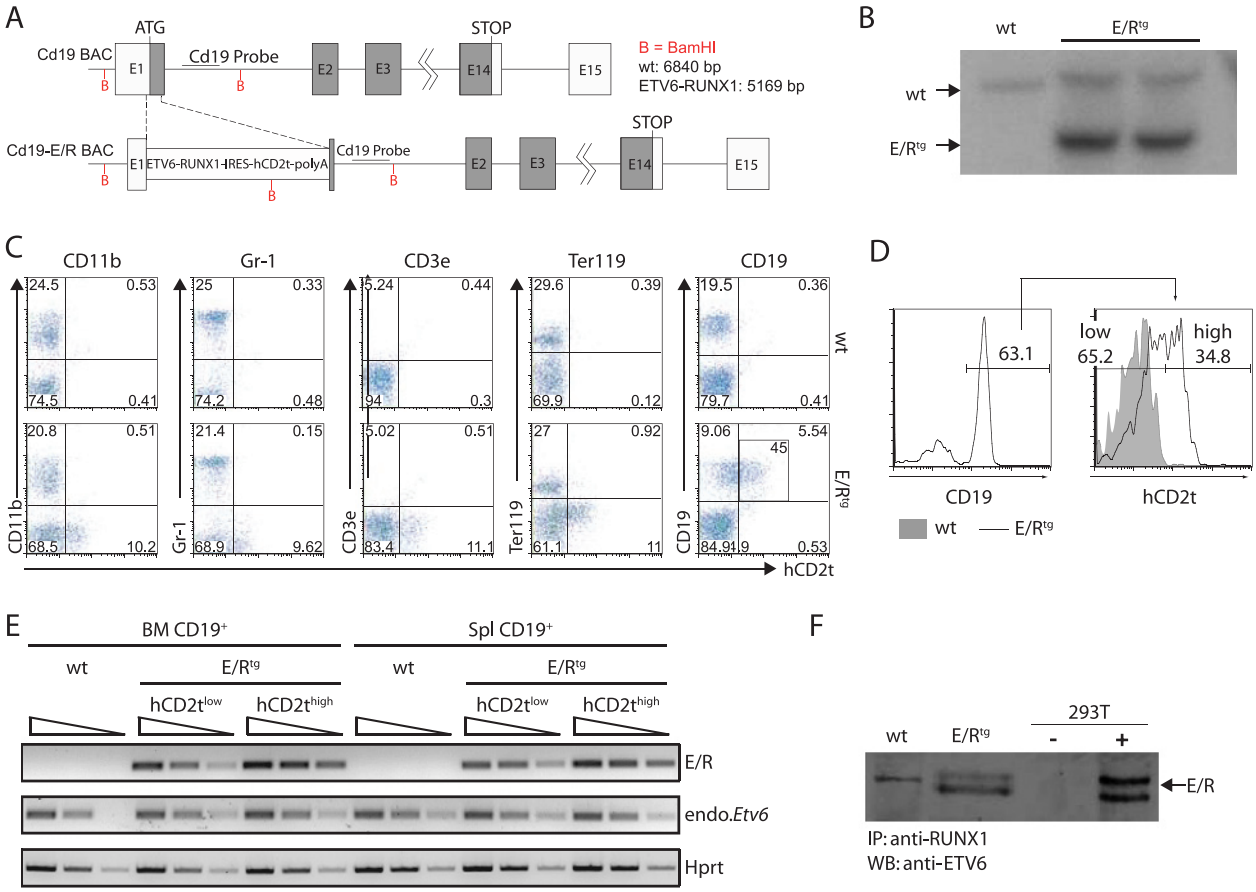

Figure 1. Design of BAC and expression analysis of the *ETV6/RUNX1* transgene. (A) The ETV6/RUNX1-IRES-hCD2t expression cassette was inserted in the first exon of the *Cd19* gene. (B) Southern blot analysis of the *Cd19* locus in an *ETV6/RUNX1* founder mouse. Genomic DNA was digested with *Bam*HI, blotted on a nitrocellulose membrane, and hybridized with a radiolabeled DNA probe against the proximal region of the *Cd19* intron 1. The expected insertion of the ETV6/RUNX1-IRES-hCD2t-polyA cassette gives rise to a labeled DNA fragment of 5169 bp in contrast to the wt *Cd19* allele (6840 bp). (C) The reporter hCD2t is specifically expressed in CD19$^+$ cells. BM cells of wt mice (upper panel) and E/R-expressing mice (lower panel) were isolated, stained for surface markers CD11b, Gr1, CD3e, Ter119 as well as CD19, and analyzed by flow cytometry. The reporter gene *hCD2t* is only expressed in CD19$^+$ cells but not in other hematopoietic lineages. Black inlet shows percentage of hCD2t$^+$ cells from the CD19-expressing population. (D) Distribution of the hCD2t expression levels on the entire CD19$^+$ cell fraction. One representative histogram of hCD2t$^{high/low}$-expressing CD19$^+$ cells is shown. (E) mRNA expression analysis for *ETV6/RUNX1* and *Etv6* in semiquantitative reverse transcription–PCR in FACS-sorted hCD2t$^{low/high}$ cells of the BM and the spleen of wt and E/R^{tg} mice. The wedge shows five-fold dilution series. (F) *ETV6/RUNX1* protein expression was analyzed by immunoprecipitation (anti-RUNX1) and Western blot analysis (anti-ETV6) from E/R^{tg} and wt fetal liver–derived B cell lines. As control, 293T cells transiently transfected with an E/R-expressing plasmid were used. An unspecific antibody cross-hybridization signal is visible in some of the samples (wt).

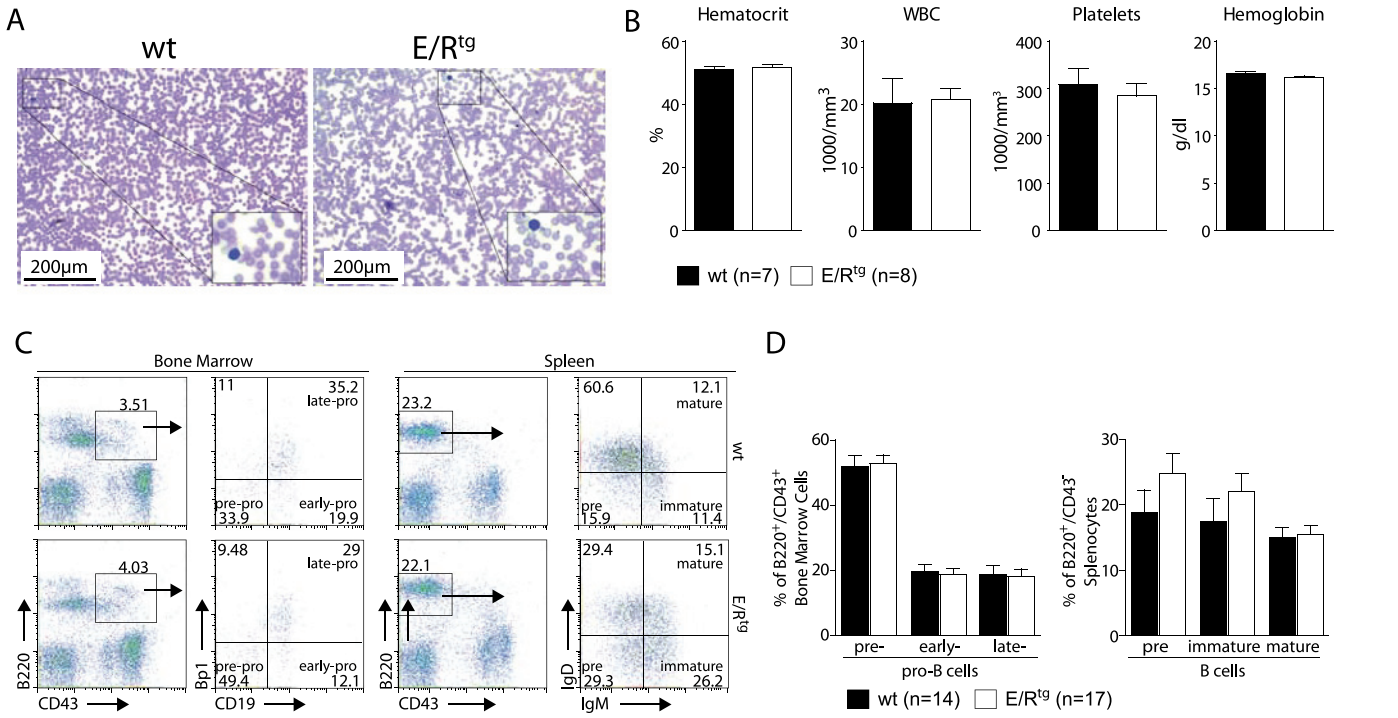

Figure 2. Effects of ETV6/RUNX1 expression on blood physiology and B cell development. (A) Representative blood smears of 8-week-old wt and E/R^{tg} mice. (B) Blood parameters of wt ($n = 7$) and E/R^{tg} ($n = 8$) mice as measured by scil Vet ABC. Statistical analysis using unpaired t test revealed no differences. (C) Flow cytometric analysis of B cell development. Shown are representative dot plots. Different developmental B cell stages are indicated in the quadrants of the dot plots as pre, early, and late and pre, immature, and mature. (D) Statistical analysis of B cell development of wt and E/R^{tg} mice using Student's unpaired t test. A summary of three experiments is shown.

antiserum directed against ETV6 [directed against helix-loop-helix (HLH) domain, a kind gift of Jan Cools, Center for Human Genetics, Faculty of Medicine, KU Leuven (University of Leuven; Leuven, Belgium)]. Proteins were electrophoretically resolved on an 8% polyacrylamide gel containing sodium dodecyl sulfate and transferred onto a polyvinylidene difluoride membrane (Whatman, Piscataway, NJ). Sites of antibody binding were detected using protein A–conjugated HRP (GE Healthcare, Little Chalfont, United Kingdom) with enhanced chemiluminiscence detection (GE Healthcare).

Infection of Fetal Livers and Cell Culture

Fetal liver cells of embryos (E14.5) were prepared, and single-cell suspensions were infected as previously described [33]. After outgrowth of cell lines, the cells were tested by flow cytometry for CD19 and hCD2t expression.

Transformed fetal liver and BM cells were maintained in RPMI (Sigma-Aldrich) containing 10% heat-inactivated fetal calf serum (PAA Laboratories, Pasching, Austria), 100 U/ml penicillin/streptomycin (Life Technologies, Carlsbad, CA), and 5 µM β-mercaptoethanol (Sigma-Aldrich). A010 cells that produce an ecotropic replication-deficient form of the Abelson virus were maintained in Dulbecco's modified Eagle's medium (Sigma-Aldrich) supplemented with 10% heat-inactivated fetal calf serum (PAA Laboratories), 100 U/ml L-glutamine (Life Technologies), and 100 U/ml penicillin/streptomycin (Life Technologies). Viral supernatant was prepared as previously described [33].

Comet Assay

DNA damage was detected using the CometAssay or single gel electrophoresis assay following the manufacturer's protocol (Trevigen, Gaithersburg, MD). Briefly, 10^6 cells/ml medium of freshly isolated BM cells [enriched for CD19$^+$ B cells by magnetic activated cell sorting (MACS)] were mixed 1:10 (v.v^{-1}) with low melting point agar at 38°C and immediately pipetted onto agar-covered slides. Slides were incubated at 4°C in the dark for 30 minutes, and the coverglass was removed, immersed in chilled lysis solution, and incubated again at 4°C for 60 minutes. Slides were placed in a horizontal electrophoresis chamber and electrophoresed with buffer (0.3 N NaOH and 1 mM EDTA) at 0.3 A for 20 minutes. Samples were dried and stained with CometAssay Silver Staining Kit (Trevigen). Comet tails were imaged using a model BA310 microscope (Motic, Hongkong) and quantified by TriTek CometScore (TriTek Corp, Sumerduck, VA). A minimum of 50 cells were scored per sample.

Statistics

All statistical analyses were done using GraphPad Prism 4 (San Diego, CA). Differences were assessed for statistical significance by unpaired Student's t test and one-way analysis of variance using the Tukey Multiple Comparison Test if not otherwise mentioned. Error bars represent means ± SD. P values are considered as follows: <.05: *, <.01: **, and <.001: ***.

Results

Generation of a CD19-Specific ETV6/RUNX1 Mouse

ETV6/RUNX1$^+$ BCP-ALL is characterized by the expansion of B cells expressing the D-related antigens Cd19 and CD10 (equivalent to Hardy Fraction C) [34]. To express the ETV6/RUNX1 fusion

protein in CD19$^+$ B cells, a BAC containing the *Cd19* locus was modified through homologous recombination in *Escherichia coli* [31,32]. A cassette encoding the human fusion gene *ETV6/RUNX1* linked through an IRES to a truncated human *CD2* (*hCD2t*) antigen reporter and followed by a polyadenylation signal (polyA) was inserted into the first exon of the *Cd19* gene. As a result of the recombination strategy, expression of functional *Cd19* from the BAC is prevented (Figure 1*A*). Several transgenic lines were obtained from oocyte injection of the CD19-ETV6/RUNX1 BAC. Southern blot analysis revealed that line 1, which was further analyzed in detail and used in the present study, harbors four copies of the CD19-ETV6/RUNX1 BAC (Figure 1*B*). To determine specific expression of ETV6/RUNX1 in B cells, we analyzed *hCD2t* reporter gene expression in various hematopoietic cell lineages isolated from BM by flow cytometry. hCD2t reporter expression was restricted to CD19$^+$ cells and could not be detected in any other cell type analyzed (Figure 1*C*). CD19$^+$ cell–specific expression of *ETV6/RUNX1* mRNA was further confirmed by performing real-time PCR analysis (Figure W1). The uniform expression of the *hCD2t* reporter gene within the CD19$^+$ cell population (Figure 1*D*) indicated that essentially all ETV6/RUNX1 transgene CD19$^+$ cells express the ETV6/RUNX1 fusion protein. Consistently, using semiquantitative reverse transcription–polymerase chain reaction (PCR), we detected the *ETV6/RUNX1* transgene expression both in hCD2t^{high} and hCD2t^{low} populations (Figure 1*E*).

As the fusion gene is expressed under the control of the *ETV6* promoter in patients with leukemia, we also tested whether the expression levels of the *ETV6/RUNX1* transgene and the endogenous *Etv6* gene are within the same range. As depicted in Figure 1*E*, *ETV6/RUNX1* and *Etv6* genes were expressed at comparable levels in CD19$^+$hCD2t^{low} cells indicating that the transgene is expressed at a nearly physiological level. Finally, we confirmed ETV6/RUNX1 expression at protein level in CD19$^+$ B cells (Figure 1*F*).

Unaltered Hematopoiesis in E/R^{tg} Mice

ETV6/RUNX1^{tg} (E/R^{tg}) mice are born at normal mendelian ratio and do not display any gross abnormalities (Figure W2). We next tested whether the expression of ETV6/RUNX1 in the CD19$^+$ B lymphoid compartment impacts on hematopoiesis in general and on B cell development in particular. Various hematopoietic lineages of wt and E/R^{tg} mice were assessed by flow cytometry. No consistent differences

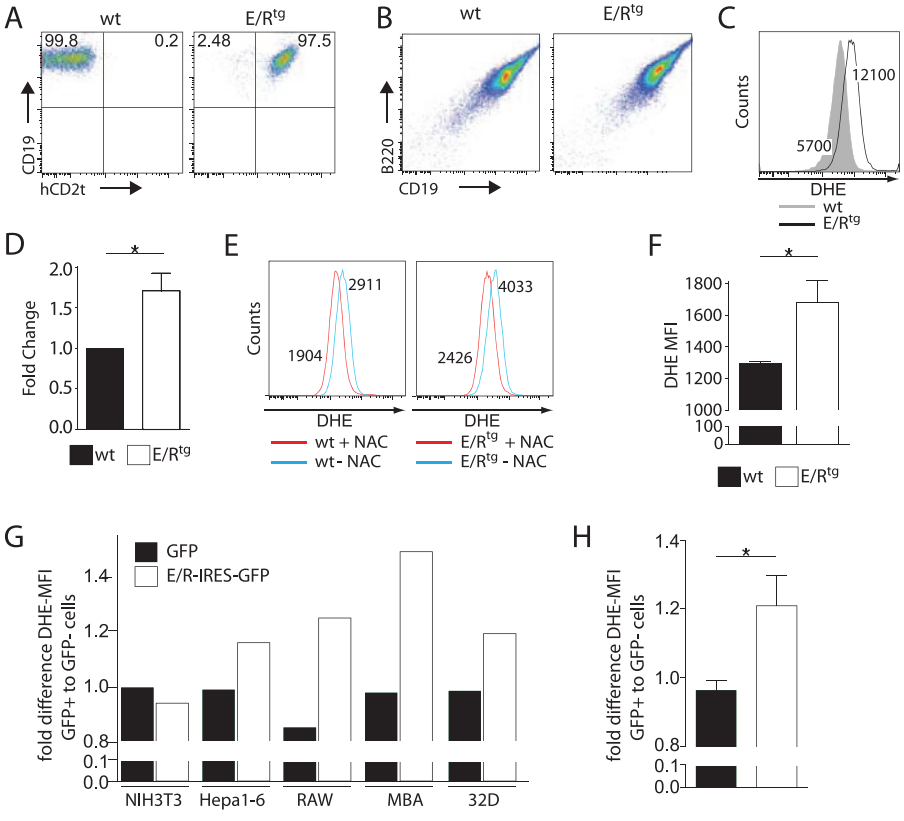

Figure 3. E/R expression induces ROS production *in vitro* and *in vivo*. (A and B) Fetal liver cells of wt and E/R^{tg} mice were infected with a retrovirus encoding for p160$^{v\text{-}ABL}$. Stably transformed pro-B cell lines were analyzed for the expression of the surface markers (A) CD19 and hCD2t as well as (B) CD19 and B220. (C) wt and E/R^{tg} cell lines were stained with DHE and subsequently analyzed by flow cytometry to measure differences in ROS level. One representative histogram is depicted. (D) A summary of all experiments using wt and E/R^{tg} cell lines stained with DHE is shown. Statistical analysis was carried out by one-tailed paired *t* test ($P = .04$). (E) wt and E/R^{tg} cell lines were treated for 24 hours with 5 mM ROS scavenger NAC and analyzed for ROS by flow cytometry. Depicted are histograms for wt (left panel) and E/R^{tg} (right panel) untreated cells and cells treated with NAC. (F) CD19$^+$ BM cells of E/R^{tg} ($n = 16$) and control littermate mice ($n = 10$) were analyzed for ROS levels. Bar graphs represent DHE-MFI ± SD; statistical differences were revealed using unpaired *t* test. (G) Indicated human and murine cell lines were transfected with a retrovirus encoding for E/R-IRES-GFP or GFP. The fold difference in DHE-MFI of GFP-positive *versus* GFP-negative cells is shown. (H) Bar graphs depict average fold change in DHE-MFI on E/R or GFP expression ± SD of all five cell lines analyzed. *$P < .05$ (unpaired *t* test).

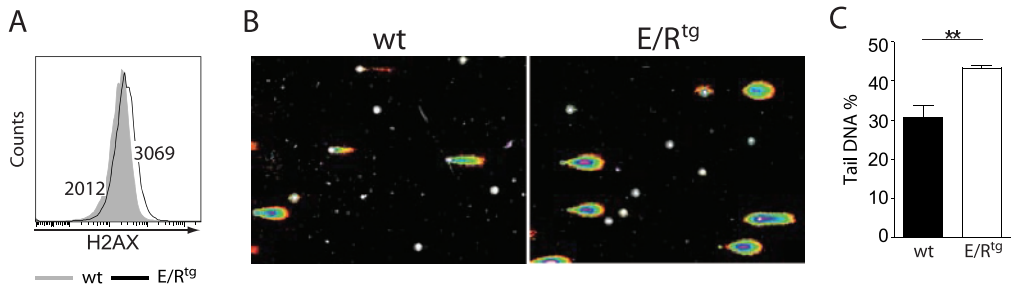

Figure 4. E/R expression induces DNA damage in wt and E/R^{tg} cells. (A) wt and E/R^{tg} cell lines were stained for γH2AX and analyzed by flow cytometry. One representative histogram is shown. (B and C) Comet assay of MACS-enriched CD19^{+} B cells derived from BM of wt and E/R^{tg} mice. Two mice of each genotype were pooled before MACS. (B) Representative pictures of comets of each genotype. (C) Statistical analysis (unpaired *t* test) of comet assay of wt and E/R^{tg} mice (n = 6 each) is depicted. Fifty pictures per sample were taken for statistical analysis of percentage of tail DNA. Average ± SD of each sample is shown.

were detected between the transgenic and control mice (Figure W3, *A* and *B*). Similarly, we failed to detect any alterations in various blood parameters that may indicate an altered blood physiology as assessed by blood smears and a hematocytometer. Briefly, no differences in hematocrit levels, white blood cell counts, platelet numbers, or hemoglobin levels were detected (Figure 2, *A* and *B*). ETV6/RUNX1^{+} ALL cells are arrested at the pro-B cell stage [26,27]. To analyze B cell development in our CD19-specific E/R^{tg} mice, we stained BM and splenocytes for B cell surface markers corresponding to distinct developmental stages (Figure 2*C*). Gating of the early B cell fractions according to Hardy in the BM revealed no significant differences in pre–pro-B cells, early pro-B cells, and late pro-B cells, respectively, between wt and E/R^{tg} mice (Figure 2*D*, *left panel*). Interestingly, we observed slightly increased pre-B cell and immature B cell numbers in the spleen of E/R^{tg} animals although mature B cells were comparable; however, this did not meet the criteria of statistical significance (Figure 2*D*, *right panel*).

ETV6/RUNX1 Elevates Cellular ROS Levels

Oncogenes such as *BCR/ABL1* induce the production of ROS [17]. To investigate whether ETV6/RUNX1 affects the equilibrium of ROS production and scavenging, we generated stable pro-B cell lines from transgenic and control mice. This allowed us to address the impact of ETV6/RUNX1 on DNA damage *in vitro* in a stable and reproducible setting. Fetal liver cells from wt and E/R^{tg} littermate embryos were infected with the Abelson virus that immortalizes pro-B cells *in vitro* [35,36]. ETV6/RUNX1 transgene expression was confirmed by surface-marker staining of the reporter gene *hCD2t* (Figure 3*A*), followed by flow cytometric analysis. No changes in the expression of the pro-B cell surface markers CD19^{+}B220^{+}CD43^{+} and the proliferation rate of the cell lines were detected upon expression of ETV6/RUNX1 when analyzed by flow cytometry and when assessed by growth curves, respectively (Figures 3*B* and W4).

Remarkably, the analysis of ROS levels in the E/R^{tg} pro-B cells consistently revealed about a two-fold increased mean fluorescence intensity (MFI) for the ROS-sensitive fluorescence probe DHE compared to control cells (wt DHE-MFI = 5700 *vs* E/R^{tg} DHE-MFI = 12,100; Figure 3, *C* and *D*). To verify that indeed an elevated ROS level accounts for the detected differences in DHE values, we treated our cells with the ROS scavenger N-acetyl-cystein (NAC) for 24 hours before measurement. A clear reduction in ROS levels was detected in E/R^{tg} as well as control cell lines (40% and 35% reduction in DHE-MFI, respectively; Figure 3*E*). To exclude the possibility of an Abelson oncogene–related impact on our experimental setup, we analyzed *ex vivo*–derived BM cells from our E/R^{tg} mice. CD19^{+} BM cells of E/R^{tg} mice (n = 16) displayed significantly elevated DHE fluorescence compared to littermate controls (n = 10; DHE-MFI = 1690 ± 138 and 1298 ± 31, respectively; P = .0365; Figure 3*F*), indicating that the observed differences are associated with ETV6/RUNX1 expression. Further evidence came from another experiment where we used five cell lines derived from different tissues of both murine and human origin (NIH3T3, HEPA1-6, RAW, MBA, and 32D). These cells were infected with a retrovirus encoding for ETV6/RUNX1-IRES-GFP or GFP alone. All cell lines tested except NIH3T3 reacted with an increase of ROS on ETV6/RUNX1 expression (P = .0285; Figure 3, *G* and *H*).

Accumulation of DNA DSBs on ETV6/RUNX1 Expression

It is a common feature of oncogenes to enhance DNA mutation rate [37]. The increased mutation rate may result from both an enhanced DNA damage and/or deregulated DNA repair mechanisms. Upon DNA DSBs, serine residue 139 of histone H2AX (γH2AX) becomes phosphorylated. This may be used as a sensitive marker to detect the presence of DSBs [38,39]. When we stained wt and E/R^{tg} cell lines with a γH2AX-specific antibody and analyzed them through intracellular flow cytometry, we found higher levels of DSBs in ETV6/RUNX1^{+} cells compared to control cells (γH2AX MFI = 3069 and 2012, respectively; Figure 4*A*). To assess DSBs in *ex vivo*–derived BM cells of wt and E/R^{tg} mice, we employed a comet assay. In such an assay, cells are embedded in agarose on microscope slides, lysed, and subjected to electrophoresis at high pH resulting in comet-like structures of the DNA. BM-derived and BM-sorted B cells were used directly *ex vivo* in this comet assay, which resulted in a higher percentage of comet tail DNA, an indicator of DNA damage, for E/R^{tg}-derived B cells compared to wt counterparts (43.3% *vs* 30.6%; Figure 4, *B* and *C*). These results suggested a link between E/R^{tg} expression and DSBs, a prerequisite for DNA mutations.

Discussion

The *ETV6/RUNX1* fusion gene has been described to arise already *in utero* [5,9,40], producing a preleukemic clone that may progress to full-blown leukemia when acquiring additional genetic alterations [5,9,11]. Here, we report the generation of a mouse model for

ETV6/RUNX1 where transgene expression is driven by a BAC containing the CD19-regulatory expression elements, restricting its expression to the B lymphoid lineage. We describe that ETV6/RUNX1-expressing B lymphoid cells display increased levels of ROS accompanied by increased DNA DSBs. Thus, we propose a model where ETV6/RUNX1 induces DNA instability through ROS deregulation, thereby facilitating mutagenesis and the appearance of additional genetic alterations.

Several reports described that enforced expression of the *ETV6/RUNX1* fusion gene from retroviral promoters impairs B cell development and induces a block at the pro-B cell stage [26], leading to the expansion of the $CD19^+$ B cell fraction [41]. Interestingly, we failed to detect any changes in B cell development at the pro-B cell stage. However, we observed a trend in elevated numbers of immature B cells as well as pre-B cells in the spleen of E/R^{tg} mice. Several reasons may account for these differences. Importantly, we succeeded in obtaining *ETV6/RUNX1* expression at similar levels when compared to the endogenous *Etv6* gene. Thus, it is attractive to speculate that higher ETV6/RUNX1 levels are required to inflict a B cell differentiation block. In addition, one may reason that the onset of transgenic expression accounts for the different impact on B cell development; it may be of relevance at which stage of B cell development the transgene is expressed. In our case, transgene expression is under the control of the *Cd19* promoter and thereby restricted to already committed B cells. In contrast, other studies employed promoters that allowed for ETV6/RUNX1 expression already at earlier developmental stages such as in hematopoietic stem and/or progenitor cells. This may support the concept that the expression of ETV6/RUNX1 before B lymphoid development is required.

ETV6/RUNX1 is commonly assumed to be the first hit during leukemogenesis, and it is assumed that secondary alterations have to occur for the clinical manifestation of the disease. In line, animal models for *ETV6/RUNX1* in mice and zebra fish revealed that the expression of the fusion gene does not suffice to allow for leukemogenesis [25–30]. Van der Weyden et al. used random mutagenesis using a Sleeping Beauty *transposon* to induce BCP-ALL in *ETV6/RUNX1* knock-in mice [42]. Several cooperating mutations were identified in these mice, some of which resembled alterations in BCP-ALL cases (including regulators of B cell development). Although a few mutations prevail, genome-wide profiling of genetic alterations in $ETV6/RUNX1^+$ BCP-ALL revealed that the mutational spectrum is highly heterogeneous, with numerous recurrent lesions generating mutations or copy number alterations in only a few patients [11,43].

Although the animal model for $ETV6/RUNX1^+$ leukemia that Van der Weyden et al. used in their study relied on the usage of knock-in mice [42], a few reports also suggest that the human *ETV6/RUNX1* gene fusion—as used for the generation of our transgenic animals—could lead to leukemia development if combined with a secondary hit in mice. It has been reported either for BM transplantation experiments where the human gene fusion was combined with loss of p16/p19 [25] or also in a recent study on inducible E/R transgenic mice in combination with loss of p16 [44] that the human fusion gene was able to induce leukemogenesis in mice.

Intracellular redox homeostasis is maintained by balancing ROS production with ROS scavenging through cellular antioxidant defense systems [45]. Several pathophysiological conditions including leukemia [46] have been associated with unbalanced ROS metabolism. Moreover, ROS is known to oxidize DNA that further provokes mutation of genes that may promote carcinogenesis [47]. In this report, we show for the first time that ETV6/RUNX1 expression in B cells is associated with elevated endogenous ROS levels and an increase in DSBs (Figures 3 and 4). The finding that a chromosomal translocation product induces DNA damage through ROS production is not entirely surprising as it has already been shown to be true for other chromosomal alterations and oncogenes; ample evidence supports this concept {summarized in [48]}. The expression of RUNX1/ETO or RUNX1 itself in human fibroblasts suffices to elevated intracellular ROS levels when compared to empty vector control [49]. These data have been supported in a *Drosophila* model where the expression of RUNX1/ETO resulted in high levels of ROS [50]. In our hands, the expression of the ETV6/RUNX1 fusion product in B cells, but also various other cell types, increased ROS levels in the respective cells. This observation also suggests that increased ROS production induced by RUNX1-containing translocation products could be a common mechanism driving leukemogenesis.

ROS is viewed as an important signaling mediator [51] and may be implicated in gene-regulatory pathways such as the one involving hypoxia-inducible factor 1 (HIF-1) [52,53]. Interestingly, ETV6/RUNX1 was shown to downregulate expression of DNA damage-inducible transcript 4 (DDIT4) (also known as REDD1), an important HIF-1 effector [54], whereas the loss of DDIT4 was reported to induce HIF-1 stabilization and tumorigenesis through a ROS-dependent mechanism [55], suggesting a possible link between ETV6/RUNX1 and increased ROS accumulation in patients.

Irradiation and topoisomerase II inhibitors are therapeutic modalities that induce DSBs [56]. This predicts that cells harboring ETV6/RUNX1 ought to be more sensitive to topoisomerase inhibitors. In fact, this prediction has been verified with patient-derived cells; BCP-ALL cells are highly sensitive to doxorubicine and etoposide, if they are $ETV6/RUNX1^+$. However, these cells do not differ from $ETV6/RUNX1^-$ BCP-ALL cells with respect to their susceptibility to other therapeutically relevant agents (vincristine, glucocorticoids, cytarabine, alkylating agents, and thioguanin) [57]. Taken together, our data propose a novel mechanism of how additional mutations could be acquired in an $ETV6/RUNX1^+$ preleukemic clone that then could cause leukemia development.

Acknowledgments

We thank Shinya Sakaguchi, Michael Freissmuth, and Richard Moriggl for continuous discussions and for critically reading the manuscript. We also thank Renate Panzer-Grümayer for providing scientific advice. We are also grateful to Hans-Christian Theussl for technical assistance in the generation of the CD19-specific E/R^{tg} mice. We also thank Reimar David, Peter Martinek as well as Jaqueline Horvath for technical assistance.

References

[1] Fears S, Gavin M, Zhang DE, Hetherington C, Ben-David Y, Rowley JD, and Nucifora G (1997). Functional characterization of *ETV6* and *ETV6/CBFA2* in the regulation of the *MCSFR* proximal promoter. *Proc Natl Acad Sci USA* **94**, 1949–1954.

[2] Fears S, Vignon C, Bohlander SK, Smith S, Rowley JD, and Nucifora G (1996). Correlation between the ETV6/CBFA2 (TEL/AML1) fusion gene and karyotypic abnormalities in children with B-cell precursor acute lymphoblastic leukemia. *Genes Chromosomes Cancer* **17**, 127–135.

[3] Golub TR, Barker GF, Bohlander SK, Hiebert SW, Ward DC, Bray-Ward P, Morgan E, Raimondi SC, Rowley JD, and Gilliland DG (1995). Fusion of the TEL gene on 12p13 to the AML1 gene on 21q22 in acute lymphoblastic leukemia. *Proc Natl Acad Sci USA* **92**, 4917–4921.

[4] Romana SP, Mauchauffé M, Le Coniat M, Chumakov I, Le Paslier D, Berger R, and Bernard OA (1995). The t(12;21) of acute lymphoblastic leukemia results in a tel-AML1 gene fusion. *Blood* **85**, 3662–3670.

[5] Greaves MF, Maia AT, Wiemels JL, and Ford AM (2003). Leukemia in twins: lessons in natural history. *Blood* **102**, 2321–2333.

[6] Greaves MF and Wiemels J (2003). Origins of chromosome translocations in childhood leukaemia. *Nat Rev Cancer* **3**, 639–649.

[7] Wiemels JL, Ford AM, Van Wering ER, Postma A, and Greaves M (1999). Protracted and variable latency of acute lymphoblastic leukemia after *TEL-AML1* gene fusion *in utero*. *Blood* **94**, 1057–1062.

[8] Maia AT, Koechling J, Corbett R, Metzler M, Wiemels JL, and Greaves M (2004). Protracted postnatal natural histories in childhood leukemia. *Genes Chromosomes Cancer* **39**, 335–340.

[9] Hong D, Gupta R, Ancliff P, Atzberger A, Brown J, Soneji S, Green J, Colman S, Piacibello W, Buckle V, et al. (2008). Initiating and cancer-propagating cells in *TEL-AML1*-associated childhood leukemia. *Science* **319**, 336–339.

[10] Castor A, Nilsson L, Astrand-Grundström I, Buitenhuis M, Ramirez C, Anderson K, Strömbeck B, Garwicz S, Békássy AN, Schmiegelow K, et al. (2005). Distinct patterns of hematopoietic stem cell involvement in acute lymphoblastic leukemia. *Nat Med* **11**, 630–637.

[11] Mullighan CG, Goorha S, Radtke I, Miller CB, Coustan-Smith E, Dalton JD, Girtman K, Mathew S, Ma J, Pounds SB, et al. (2007). Genome-wide analysis of genetic alterations in acute lymphoblastic leukaemia. *Nature* **446**, 758–764.

[12] Kuster L, Grausenburger R, Fuka G, Kaindl U, Krapf G, Inthal A, Mann G, Kauer M, Rainer J, Kofler R, et al. (2011). ETV6/RUNX1-positive relapses evolve from an ancestral clone and frequently acquire deletions of genes implicated in glucocorticoid signaling. *Blood* **117**, 2658–2667.

[13] Hanahan D and Weinberg RA (2011). Hallmarks of cancer: the next generation. *Cell* **144**, 646–674.

[14] Slupphaug G, Kavli B, and Krokan HE (2003). The interacting pathways for prevention and repair of oxidative DNA damage. *Mutat Res* **531**, 231–251.

[15] Valko M, Leibfritz D, Moncol J, Cronin MT, Mazur M, and Telser J (2007). Free radicals and antioxidants in normal physiological functions and human disease. *Int J Biochem Cell Biol* **39**, 44–84.

[16] Ziech D, Franco R, Pappa A, and Panayiotidis MI (2011). Reactive oxygen species (ROS)–induced genetic and epigenetic alterations in human carcinogenesis. *Mutat Res* **711**, 167–173.

[17] Koptyra M, Falinski R, Nowicki MO, Stoklosa T, Majsterek I, Nieborowska-Skorska M, Blasiak J, and Skorski T (2006). BCR/ABL kinase induces self-mutagenesis via reactive oxygen species to encode imatinib resistance. *Blood* **108**, 319–327.

[18] Nowicki MO, Falinski R, Koptyra M, Slupianek A, Stoklosa T, Gloc E, Nieborowska-Skorska M, Blasiak J, and Skorski T (2004). BCR/ABL oncogenic kinase promotes unfaithful repair of the reactive oxygen species–dependent DNA double-strand breaks. *Blood* **104**, 3746–3753.

[19] Sallmyr A, Fan J, Datta K, Kim KT, Grosu D, Shapiro P, Small D, and Rassool F (2008). Internal tandem duplication of FLT3 (FLT3/ITD) induces increased ROS production, DNA damage, and misrepair: implications for poor prognosis in AML. *Blood* **111**, 3173–3182.

[20] Walz C, Crowley BJ, Hudon HE, Gramlich JL, Neuberg DS, Podar K, Griffin JD, and Sattler M (2006). Activated Jak2 with the V617F point mutation promotes G_1/S phase transition. *J Biol Chem* **281**, 18177–18183.

[21] Burke BA and Carroll M (2010). BCR–ABL: a multi-faceted promoter of DNA mutation in chronic myelogeneous leukemia. *Leukemia* **24**, 1105–1112.

[22] Alcalay M, Meani N, Gelmetti V, Fantozzi A, Fagioli M, Orleth A, Riganelli D, Sebastiani C, Cappelli E, Casciari C, et al. (2003). Acute myeloid leukemia fusion proteins deregulate genes involved in stem cell maintenance and DNA repair. *J Clin Invest* **112**, 1751–1761.

[23] Krejci O, Wunderlich M, Geiger H, Chou FS, Schleimer D, Jansen M, Andreassen PR, and Mulloy JC (2008). p53 signaling in response to increased DNA damage sensitizes AML1-ETO cells to stress-induced death. *Blood* **111**, 2190–2199.

[24] Krapf G, Kaindl U, Kilbey A, Fuka G, Inthal A, Joas R, Mann G, Neil JC, Haas OA, and Panzer-Grümayer ER (2010). ETV6/RUNX1 abrogates mitotic checkpoint function and targets its key player MAD2L1. *Oncogene* **29**, 3307–3312.

[25] Bernardin F, Yang Y, Cleaves R, Zahurak M, Cheng L, Civin CI, and Friedman AD (2002). TEL-AML1, expressed from t(12;21) in human acute lymphocytic leukemia, induces acute leukemia in mice. *Cancer Res* **62**, 3904–3908.

[26] Tsuzuki S, Seto M, Greaves M, and Enver T (2004). Modeling first-hit functions of the t(12;21) *TEL-AML1* translocation in mice. *Proc Natl Acad Sci USA* **101**, 8443–8448.

[27] Fischer M, Schwieger M, Horn S, Niebuhr B, Ford A, Roscher S, Bergholz U, Greaves M, Löhler J, and Stocking C (2005). Defining the oncogenic function of the TEL/AML1 (*ETV6/RUNX1*) fusion protein in a mouse model. *Oncogene* **24**, 7579–7591.

[28] Sabaawy HE, Azuma M, Embree LJ, Tsai HJ, Starost MF, and Hickstein DD (2006). *TEL-AML1* transgenic zebrafish model of precursor B cell acute lymphoblastic leukemia. *Proc Natl Acad Sci USA* **103**, 15166–15171.

[29] Schindler JW, Van Buren D, Foudi A, Krejci O, Qin J, Orkin SH, and Hock H (2009). TEL-AML1 corrupts hematopoietic stem cells to persist in the bone marrow and initiate leukemia. *Cell Stem Cell* **5**, 43–53.

[30] Andreasson P, Schwaller J, Anastasiadou E, Aster J, and Gilliland DG (2001). The expression of *ETV6/CBFA2* (*TEL/AML1*) is not sufficient for the transformation of hematopoietic cell lines *in vitro* or the induction of hematologic disease *in vivo*. *Cancer Genet Cytogenet* **130**, 93–104.

[31] Delogu A, Schebesta A, Sun Q, Aschenbrenner K, Perlot T, and Busslinger M (2006). Gene repression by Pax5 in B cells is essential for blood cell homeostasis and is reversed in plasma cells. *Immunity* **24**, 269–281.

[32] Muyrers JP, Zhang Y, Testa G, and Stewart AF (1999). Rapid modification of bacterial artificial chromosomes by ET-recombination. *Nucleic Acids Res* **27**, 1555–1557.

[33] Sexl V, Piekorz R, Moriggl R, Rohrer J, Brown MP, Bunting KD, Rothammer K, Roussel MF, and Ihle JN (2000). Stat5a/b contribute to interleukin 7–induced B-cell precursor expansion, but *abl*- and *bcr/abl*-induced transformation are independent of Stat5. *Blood* **96**, 2277–2283.

[34] Romana SP, Poirel H, Leconiat M, Flexor MA, Mauchauffé M, Jonveaux P, Macintyre EA, Berger R, and Bernard OA (1995). High frequency of t(12;21) in childhood B-lineage acute lymphoblastic leukemia. *Blood* **86**, 4263–4269.

[35] Witte ON (1986). Functions of the abl oncogene. *Cancer Surv* **5**, 183–197.

[36] Rosenberg N and Witte ON (1988). The viral and cellular forms of the Abelson (abl) oncogene. *Adv Virus Res* **35**, 39–81.

[37] Skorski T (2002). BCR/ABL regulates response to DNA damage: the role in resistance to genotoxic treatment and in genomic instability. *Oncogene* **21**, 8591–8604.

[38] Paull TT, Rogakou EP, Yamazaki V, Kirchgessner CU, Gellert M, and Bonner WM (2000). A critical role for histone H2AX in recruitment of repair factors to nuclear foci after DNA damage. *Curr Biol* **10**, 886–895.

[39] Rogakou EP, Pilch DR, Orr AH, Ivanova VS, and Bonner WM (1998). DNA double-stranded breaks induce histone H2AX phosphorylation on serine 139. *J Biol Chem* **273**, 5858–5868.

[40] Mori H, Colman SM, Xiao Z, Ford AM, Healy LE, Donaldson C, Hows JM, Navarrete C, and Greaves M (2002). Chromosome translocations and covert leukemic clones are generated during normal fetal development. *Proc Natl Acad Sci USA* **99**, 8242–8247.

[41] Morrow M, Horton S, Kioussis D, Brady HJ, and Williams O (2004). TEL-AML1 promotes development of specific hematopoietic lineages consistent with pre-leukemic activity. *Blood* **103**, 3890–3896.

[42] van der Weyden L, Giotopoulos G, Rust AG, Matheson LS, van Delft FW, Kong J, Corcoran AE, Greaves MF, Mullighan CG, Huntly BJ, et al. (2011). Modeling the evolution of *ETV6-RUNX1*–induced B-cell precursor acute lymphoblastic leukemia in mice. *Blood* **118**, 1041–1051.

[43] Lilljebjörn H, Soneson C, Andersson A, Heldrup J, Behrendtz M, Kawamata N, Ogawa S, Koeffler HP, Mitelman F, Johansson B, et al. (2010). The correlation pattern of acquired copy number changes in 164 *ETV6/RUNX1*-positive childhood acute lymphoblastic leukemias. *Hum Mol Genet* **19**, 3150–3158.

[44] Li M, Jones L, Gaillard C, Binnewies M, Ochoa R, Garcia E, Lam V, Wei G, Yang W, Lobe C, et al. (2013). Initially disadvantaged, TEL-AML1 cells expand and initiate leukemia in response to irradiation and cooperating mutations. *Leukemia* **27**, 1570–1573.

[45] Nguyen T, Nioi P, and Pickett CB (2009). The Nrf2-antioxidant response element signaling pathway and its activation by oxidative stress. *J Biol Chem* **284**, 13291–13295.

[46] Suh YA, Arnold RS, Lassegue B, Shi J, Xu X, Sorescu D, Chung AB, Griendling KK, and Lambeth JD (1999). Cell transformation by the superoxide-generating oxidase Mox1. *Nature* **401**, 79–82.

[47] Shibutani S, Takeshita M, and Grollman AP (1991). Insertion of specific bases during DNA synthesis past the oxidation-damaged base 8-oxodG. *Nature* **349**, 431–434.

[48] Skorski T (2011). Chronic myeloid leukemia cells refractory/resistant to tyrosine kinase inhibitors are genetically unstable and may cause relapse and malignant progression to the terminal disease state. *Leuk Lymphoma* **52**(suppl 1), 23–29.

[49] Wolyniec K, Wotton S, Kilbey A, Jenkins A, Terry A, Peters G, Stocking C, Cameron E, and Neil JC (2009). RUNX1 and its fusion oncoprotein derivative, RUNX1-ETO, induce senescence-like growth arrest independently of replicative stress. *Oncogene* **28**, 2502–2512.

[50] Sinenko SA, Hung T, Moroz T, Tran QM, Sidhu S, Cheney MD, Speck NA, and Banerjee U (2010). Genetic manipulation of AML1-ETO–induced expansion of hematopoietic precursors in a *Drosophila* model. *Blood* **116**, 4612–4620.

[51] Thannickal VJ and Fanburg BL (2000). Reactive oxygen species in cell signaling. *Am J Physiol Lung Cell Mol Physiol* **279**, L1005–L1028.

[52] Chandel NS, McClintock DS, Feliciano CE, Wood TM, Melendez JA, Rodriguez AM, and Schumacker PT (2000). Reactive oxygen species generated at mitochondrial complex III stabilize hypoxia-inducible factor-1α during hypoxia: a mechanism of O_2 sensing. *J Biol Chem* **275**, 25130–25138.

[53] Goyal P, Weissmann N, Grimminger F, Hegel C, Bader L, Rose F, Fink L, Ghofrani HA, Schermuly RT, Schmidt HH, et al. (2004). Upregulation of NAD(P)H oxidase 1 in hypoxia activates hypoxia-inducible factor 1 via increase in reactive oxygen species. *Free Radic Biol Med* **36**, 1279–1288.

[54] Fuka G, Kauer M, Kofler R, Haas OA, and Panzer-Grümayer R (2011). The leukemia-specific fusion gene *ETV6/RUNX1* perturbs distinct key biological functions primarily by gene repression. *PloS One* **6**, e26348.

[55] Horak P, Crawford AR, Vadysirisack DD, Nash ZM, DeYoung MP, Sgroi D, and Ellisen LW (2010). Negative feedback control of HIF-1 through REDD1-regulated ROS suppresses tumorigenesis. *Proc Natl Acad Sci USA* **107**, 4675–4680.

[56] Curtin NJ (2012). DNA repair dysregulation from cancer driver to therapeutic target. *Nat Rev Cancer* **12**, 801–817.

[57] Frost BM, Forestier E, Gustafsson G, Nygren P, Hellebostad M, Jonsson OG, Kanerva J, Schmiegelow K, Larsson R, and Lönnerholm G (2004). Translocation t(12;21) is related to *in vitro* cellular drug sensitivity to doxorubicin and etoposide in childhood acute lymphoblastic leukemia. *Blood* **104**, 2452–2457.

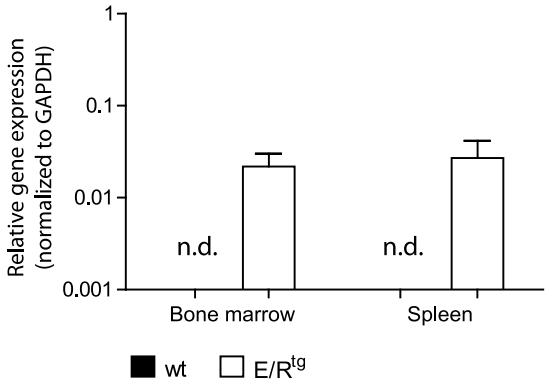

Figure W1. ETV6/RUNX1 is specifically expressed in CD19$^+$ B cells of E/R^{tg} mice. BM and spleen of wt and E/R^{tg} mice ($n = 3$ each) were analyzed for ETV6/RUNX1 mRNA expression by real-time PCR. Depicted are means ± SD. The SYBR green method was used for quantification of the PCR product. Sequences of primer pairs used were given as follows (5′-3′): *ETV6/RUNX1*, forward—CTCTGTCTCCCCGCCTGAA and reverse—CGGCTCGTGCTGGCAT; mouse *gapdh*, forward—5′-AGAAGGTGGTGAAGCAGGCATC-3′ and reverse—5′-CGGCATCGAAGGTGGAAGAGTG-3′.

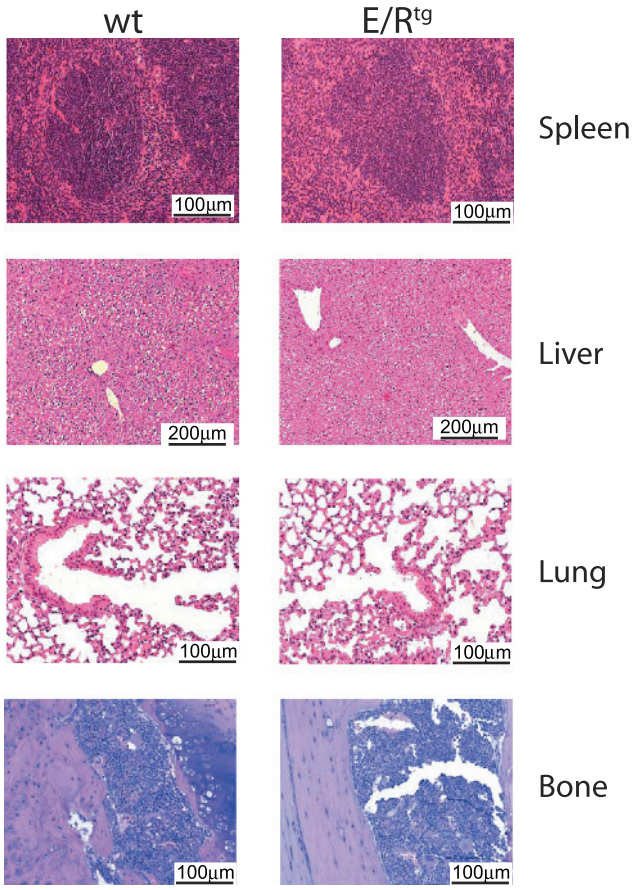

Figure W2. The expression of ETV6/RUNX1 in the CD19$^+$ B lymphoid compartment does not lead to gross abnormalities in hematopoietic/lymphatic organs. Representative examples of hematoxylin and eosin (H&E)-stained sections of spleen (top panel), liver (second panel), lung (third panel), and bone (fourth panel) of wt and E/R^{tg} mice are depicted. Spleens, livers, lungs, and bone were fixed with 4% paraformaldehyde for 24 hours, dehydrated, and embedded in paraffin. After fixation, the bones were additionally decalcified in EDTA. Sections (5 Am) were stained with H&E using standard protocols. Images were taken using a Carl Zeiss Axio Imager.Z1 microscope.

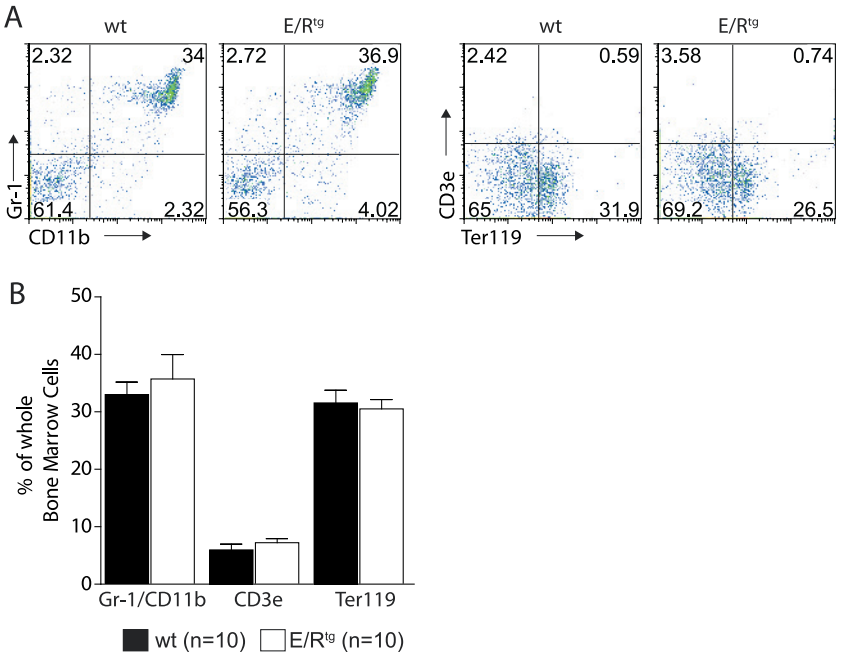

Figure W3. The expression of ETV6/RUNX1 in the CD19$^+$ B lymphoid compartment does not affect hematopoietic lineages other than the B cell lineage. (A) BM of wt and E/R^{tg} mice was analyzed for myeloid, T-lymphoid, and erythroid lineage markers by flow cytometry. Representative dot plot diagrams are depicted. (B) Bar graphs depict statistical analysis of hematopoietic lineages of wt and E/R^{tg} mice. Percentages of Gr-1/CD11b$^+$, CD3e$^+$, and Ter119$^+$ cells in whole BM are shown. No consistent differences were detected between the transgenic and control mice as analyzed by unpaired *t* test.

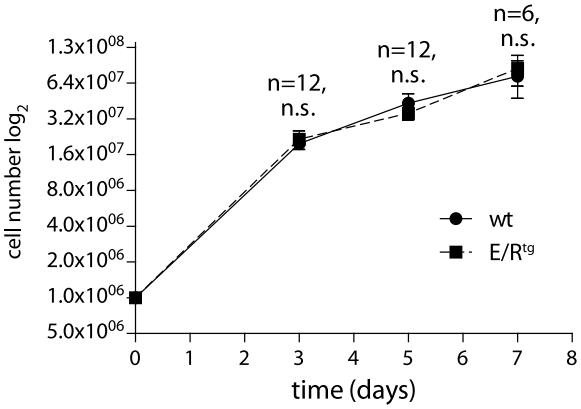

Figure W4. E/R transgenic cells proliferate with similar kinetics as wt controls. An amount of 10^6 cells of the E/R^{tg} and wt cell lines, respectively, was plated, and total cell numbers were determined after indicated days. The increase in cell number is shown in the graph. The experiment was performed more than three times. A summary of the experiment is depicted. Data points show means of 12 or 6 (as indicated), and whiskers represent SE. We did not observe significant differences in growth between the cell lines as analyzed by unpaired *t* test for each time point.